A Throughput Fast Measurement Method for Two-Antenna Equipped Wireless MIMO Terminals

Penghui Shen, *Member, IEEE*, Quan Yu, *Fellow, IEEE*, Daryl G. Beetner, *Senior Member, IEEE*, and Yihong Qi, *Fellow, IEEE*

***Abstract*— According to the third Generation Partnership Project specification, a period of 8–12.8 h is required to evaluate the multiple-input–multiple-output (MIMO) performance of a wireless terminal for a single frequency point and channel model combination. The following article proposes a semi-simulation, semi-measurement-based MIMO throughput modeling scheme which can reduce the 8–12.8-h measurement time to 40–60 min, corresponding to more than a ten times improvement of the test efficiency, without loss of the test accuracy.**

***Index Terms*— Multiple-input–multiple-output (MIMO), semi-simulation semi-measurement, throughput measurement.**

I. Introduction

MULTIPLE-INPUT–MULTIPLE-OUTPUT (MIMO) technology is the basic default for 4G, 5G, and beyond wireless terminals [1], [2], [3]. The goal of the multi-antenna is to obtain a greater data transmission rate [4], [5]. For terminals with limited size (such as cell phones, routers, smartwatches, and TV sets), however, cross-coupling and correlation problems between the multi-antennas may cause the communication rate to drop dramatically [6], [7]. The third Generation Partnership Project (3GPP) and the Cellular Telecommunications Industry Association (CTIA) have provided standards for MIMO terminal network access testing, in which 2–7 channel models are specified for evaluating the throughput performance [8], [9], [10], [11]. The test results are specified to determine whether the terminal meets the network assessment requirements.

MIMO over-the-air (OTA) testing has been developed over a dozen years, among which the reverberation chamber (RC) method [12], [13], [14], the multiple probe anechoic chamber (MPAC) method [15], [16], [17], the conducted two-step (CTS) method [18], [19], and the radiation two-step method (RTS) have been presented [5], [6], [7], [10]. The RC method uses an RC to simulate a multiple-path channel environment, and some schemes also have a channel emulator involved. The MPAC method uses one probe ring to simulate a 2-D channel model or three probe rings to simulate a 3-D channel environment. The 3-D distribution probes in MPAC simulate the signal angles of arrival (AoAs), and each of the probes links a channel simulation circuit to realize the fading, delay, and Doppler. The idea of the CTS combines the channel information and antenna pattern to obtain the throughput test signals via computing and then feed them to the receivers through the radio frequency (RF) cables. Due to a lack of consideration of noise interference in CTS, the result may not be correct. Furthermore, the RTS was proposed, where an inverse matrix was used to build the OTA direct connect. MPAC and RTS were introduced into the 3GPP test specification (TS) 37.544 and CTIA test plan [8], [9], [10], [11].

Performing a throughput measurement, however, is extremely time-consuming. According to the standards [8], [9], [10], [11], a period of 8–12.8 h is required to evaluate the MIMO performance of a terminal at a single combination of the test frequency and the selected channel model. A general wireless terminal can support 3–8 bands, in which three frequency points (high, middle, and low-frequency points) are to be measured. At least seven-channel models [spatial channel model extension (SCME), urban macro (UMa), and urban micro (UMi), clustered delay line (CDL) A, B, C, D, and E channel models] must be considered [10], [20], [21], [22], [23]. Thus, to comprehensively evaluate the MIMO performance of a terminal under all cases requires at least 3 (bands) $\times$ 3 (frequency points) $\times$ 7 (channel models) $\times$ 8 (hours) $=$ 504 h. Even worse, the number of wireless terminals is enormous and has the potential to grow explosively with the promotion of 5G, the Internet of Things (IoT), and vehicle-to-everything (V2X) technology [24], [25], [26]. These factors will result in an astronomical amount of testing time.

To address the issues, this article proposes a fast MIMO throughput test scheme for two-antenna equipped user equipment (UE) operating at 2 $\times$ 2 MIMO mode, which predicts the terminal throughput performance under different test cases based on the selected channel model and the UE RF performance information. The proposed method can shorten the required 8–12.8 h of measurement time to 40–60 min and

Manuscript received 27 June 2022; revised 16 September 2022; accepted 6 October 2022. Date of publication 16 February 2023; date of current version 22 February 2023. This work was supported by the China Postdoctoral Science Foundation under Grant 2021M691679. The Associate Editor coordinating the review process was Zhengyu Peng. *(Corresponding author: Quan Yu.)*

Penghui Shen, Quan Yu, and Yihong Qi are with the Peng Cheng Laboratory, Shenzhen 518066, China (e-mail: spenghui.shen@generaltest.com; quanyu@ieee.org; yihong.qi@generaltest.com).

Daryl G. Beetner is with the Electrical and Computer Engineer Department, Missouri University of Science and Technology, Rolla, MO 65409 USA (e-mail: daryl@mst.edu).

Digital Object Identifier 10.1109/TIM.2022.3216069

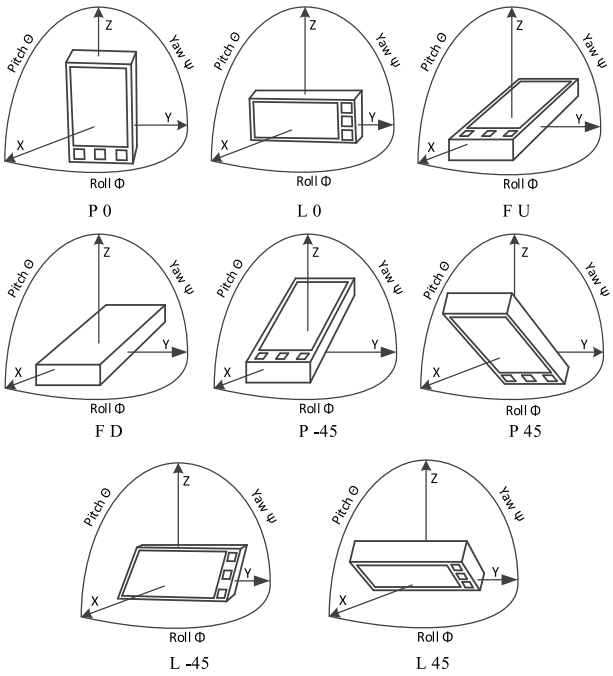

Fig. 1. Eight different test postures under a selected channel model for MIMO throughput test.

TABLE I
EXPLANATION OF THE EIGHT TEST POSTURES

posing postures	Explanations
P 0	Portrait orientation
L 0	Landscape orientation
F U	Face up
F D	Face down
P -45	Portrait orientation with -45 degrees rotation
P 45	Portrait orientation with 45 degrees rotation
L -45	Landscape orientation with -45 degrees rotation
L 45	Landscape orientation with 45 degrees rotation

can do so without loss of test accuracy. For size-constrained wireless terminals (e.g., IoT, V2X, and most mobile terminals), a dual-antenna configuration is cost-effective and common. The proposed method can solve the discussed time-consuming test problem for such a large number of terminals.

II. STANDARD MIMO THROUGHPUT EVALUATION PROCEDURE

The SCME channel model, which has been widely utilized in the 3GPP and CTIA standards, is introduced as an example to illustrate the standard test procedure and time overhead. According to the standards [10], the wireless UE must be evaluated in eight different postures under a selected channel model, as shown in Fig. 1 and explained in Table I.

It should be noted that SCME was initially proposed as a 3-D channel model, which describes the incoming wave information from all angles of space to the terminal [21], [22], [23]. However, since the MPAC method has difficulties in simulating 3-D channel models, in the current standards,

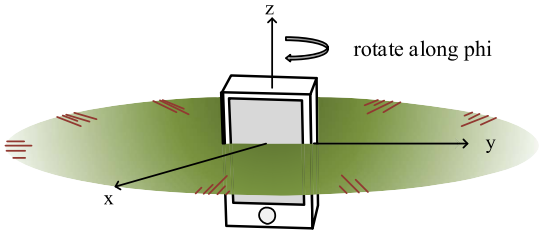

Fig. 2. Signal arrival directions in the SCME channel model defined in the 3GPP standard are on a 2-D plane.

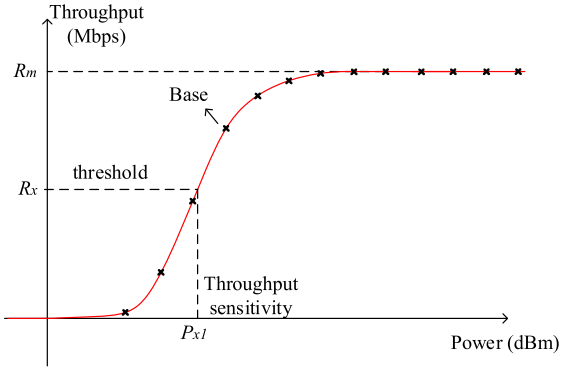

Fig. 3. General relationship between throughput and downlink power.

SCME channel models are simplified to 2-D, and all AoAs are defined in the same plane, as shown in Fig. 2. To comprehensively evaluate the performance of the DUT is necessary to traverse the postures that might be used by the DUT as much as possible during testing. This need is the reason why eight postures are specified in the standards [10].

To account for the fact that the DUT throughput performance will differ with the DUT orientation relative to the channel model, it is necessary to rotate the DUT along the direction perpendicular to the 2-D channel model plane in each posture, as shown in Fig. 2. Measurements in 30° steps are specified from 0 to 360 degrees along the phi axis, which corresponds to a total of 12 rotations. For each rotation, a downlink-power-throughput curve is measured. A total of 1 (frequency point) × 1 (channel model) × 8 (postures) × 12 (curves) = 96 curve tests are required to characterize a single frequency point and channel model.

The relationship between throughput and downlink power is illustrated by the red baseline in Fig. 3, where the communication rate is measured while reducing the downlink power step by step until the throughput falls below a certain preset value (e.g., 20% of the maximum value). With each downlink power level, a certain number of data blocks are used to determine the communication bit error rate (BER), as shown in Fig. 3. The black "X" marks in Fig. 3 are the points obtained from the actual test and the red line is the throughput-downlink power curve found using the measured points. Typically, each curve requires 5–8 min to measure, corresponding to a total test time of 8–12.8 h for just one combination of a single channel model and a frequency point [10].

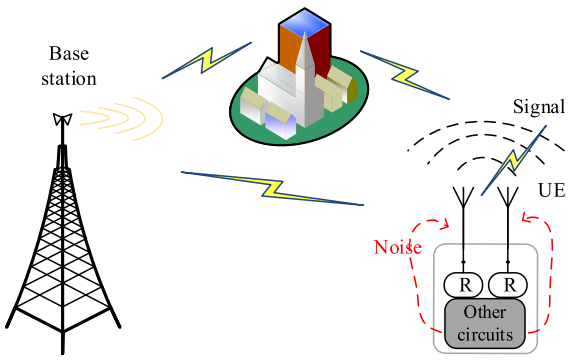

Fig. 4. MIMO signal transmission demonstration diagram including multi-path.

III. Theoretical Foundations

This article proposes a half-simulation and half-test-based UE MIMO throughput accessing model. As shown in Fig. 4, the multi-stream signal from the base station (BS) reaches the antenna front of the MIMO terminal after crossing the spatial multipath channel and is then delivered to the receiver via the antennas. In addition to the intended signal, the RF noise radiated by the UE itself may also be coupled into the receivers through the antennas or other mechanisms. As shown in [27], the signal received by the MIMO terminal receiver can be expressed as

$$\begin{aligned} y(t) &= H(t)x(t) + n(t) \\ y_z(t) &= H(t)x(t) \end{aligned} \tag{1}$$

where $x(t)$ and $y_z(t)$ denote the transmitted signal vector and the received signal vector (without noise), respectively; $n(t)$ is the coupled noise vector; and $H(t)$ is the defined channel coefficient matrix [27], which contains information about the BS antenna patterns, the channel model, and the UE antenna patterns. The (l, k) component (in row l, column k) of $H(t)$, denoted by $h_{l,k}(t)$, can be written as

$$h_{l,k}(t) = \sum_{n=1}^{N} h_{l,k,n}(t) \tag{2}$$

where $h_{l,k,n}(t)$ is the transmission parameter from the input of the kth BS antenna to the input of the lth terminal receiver under the nth channel path. For the sake of generality, $h_{l,k,n}(t)$ can be expressed as [27]

$$h_{l,k,n}(t) = e^{\varphi(t)} \begin{bmatrix} F^{v}_{u,\mathrm{UE}}\left(\varphi^{(n)}_{\mathrm{AoA}}\right) \\ F^{h}_{u,\mathrm{UE}}\left(\varphi^{(n)}_{\mathrm{AoA}}\right) \end{bmatrix}^{\mathrm{T}} * \begin{bmatrix} \chi^{v,v}_{n} & \chi^{v,h}_{n} \\ \chi^{h,v}_{n} & \chi^{h,h}_{n} \end{bmatrix} * \begin{bmatrix} F^{v}_{s,\mathrm{BS}}\left(\varphi^{(n)}_{\mathrm{AoD}}\right) \\ F^{h}_{s,\mathrm{BS}}\left(\varphi^{(n)}_{\mathrm{AoD}}\right) \end{bmatrix} \tag{3}$$

where $e^{\varphi(t)}$ is the phase factor which includes the Doppler effect, phase, and delay of the nth path; $\varphi^{(n)}_{\mathrm{AoA}}$, $\varphi^{(n)}_{\mathrm{AoD}}$, and $\chi^{x,y}_{n}$ represent the angle of arrival, angle of departure, and complex amplitude phase change from y to x polarization in the nth path, respectively; $F^{v}_{u,\mathrm{UE}}(\varphi^{(n)}_{\mathrm{AoA}})$ and $F^{v}_{s,\mathrm{BS}}(\varphi^{(n)}_{\mathrm{AoD}})$ are the gain of the UE uth antenna; and $[\,]^{\mathrm{T}}$ denotes matrix transpose. Equations (1)–(3) describe the stream transmissions of MIMO communications from the BS to the terminal, which also corresponds to the basic theory behind the MIMO throughput test. The channel model and the BS antenna pattern is known and specified in the standard [10], and the UE antenna pattern can be measured. The channel correlation matrixes can therefore be simulated before performing throughput curve tests, which is the basic premise of the model, as discussed below.

As discussed earlier, a total of 96 throughput curves are required to characterize a single combination of channel model and frequency. The receivers and the front-end noise remain fixed among all of these measurements. Only the channel correlation matrix changes (due to the change of the orientation of the DUT to the channel model). The proposed modeling can thus be performed in two steps. The first step is to obtain a throughput-downlink power curve for a single frequency and channel model through step-by-step testing to determine the receiver's underlying response for multi-stream signals. The second step is to simulate and compute the difference in throughput performance of MIMO terminals when loaded with different channel correlation matrices. The model thus achieves the evaluation of the entire MIMO throughput performance via just one test plus 95 simulations.

The impact on throughput caused by the channel correlation matrix in this model is illustrated below using 2×2 MIMO as an example. The channel correlation matrix is composed of four components

$$H(t) = \begin{bmatrix} h_{1,1}(t) & h_{1,2}(t) \\ h_{2,1}(t) & h_{2,2}(t) \end{bmatrix} \tag{4}$$

where $h_{l,k}(t)$ represents the signal amplitude and phase conversion from the kth transmitter port of the BS to the lth receiver port of the UE. In this article, we consider the modeling of this 2×2 MIMO in terms of both spatial and temporal properties [28]. The study [28] proposes an analysis model of MIMO throughput performance, in which the MIMO performance can be decomposed into various indicators, such as antenna gains of all antennas, efficiencies, correlation, receiver noise, receiver TIS, receiver balance, and time-domain correlation coefficient. Based on the concept that MIMO performance can be decomposed into various impact factors, this article presents a fast MIMO measurement methodology and procedure for MIMO performance. The proposed fast test method focuses on solving the problem of how to improve the measurement speed, and without reducing the test accuracy.

A. Spatial Properties of $H(t)$

The spatial characteristics of $H(t)$ correspond to the attenuation of the signal during transmission. Obviously, the greater the spatial path loss, the weaker the signal received by the UE and the worse the throughput performance. In the model developed here, the attenuation factor of the signal

is defined as [28]

$$G_m = 10\lg\left(\frac{E\left[\left|h_{1,1}(t)\right|^2\right]+E\left[\left|h_{1,2}(t)\right|^2\right]}{2} + \frac{E\left[\left|h_{2,1}(t)\right|^2\right]+E\left[\left|h_{2,2}(t)\right|^2\right]}{2}\right) \quad (5)$$

where $E[\ ]$ denotes mathematical expectation over time, and $|\ |$ is the absolute value.

Another factor to be considered is the condition number of the channel correlation matrix. It is known that the deterioration of the matrix condition number can seriously affect the signal-to-noise ratio of the demodulated signal, which in turn affects the channel estimation and demodulation of MIMO. The throughput impact factor due to the matrix condition number is defined in the model as (in the format of dB) [28]

$$G_f = 10\lg\left(\text{norm}\left(\begin{bmatrix}\frac{1}{f_m} & 0\\ 0 & f_m\end{bmatrix}, 2\right)\right) \quad (6)$$

where

$$f_m = \sqrt[4]{\frac{E\left[\left|h_{2,1}(t)\right|^2\right]+E\left[\left|h_{2,2}(t)\right|^2\right]}{E\left[\left|h_{1,1}(t)\right|^2\right]+E\left[\left|h_{1,2}(t)\right|^2\right]}} \quad (7)$$

and where $\text{norm}\left(\begin{bmatrix}1/f_m & 0\\ 0 & f_m\end{bmatrix}, 2\right)$ denotes the second normal number.

B. Temporal Property of $H(t)$

The signal time-domain correlation can be indicated using the correlation coefficient of the channel correlation matrix, which is defined as [28]

$$\rho^t = \sqrt{\frac{E\left[\left|h_{1,1}(t)h_{1,2}^*(t)\right|\right]E\left[\left|h_{2,1}(t)h_{2,2}^*(t)\right|\right]}{N\_h(t)}} \quad (8a)$$

$$\rho^r = \sqrt{\frac{E\left[\left|h_{1,1}(t)h_{2,1}^*(t)\right|\right]E\left[\left|h_{1,2}(t)h_{2,2}^*(t)\right|\right]}{N\_h(t)}} \quad (8b)$$

where

$$N_{h(t)} = \prod_{i=1}^{2}\prod_{j=1}^{2}\sqrt{E\left[\left|h_{i,j}(t)\right|^2\right]}. \quad (9)$$

Then, ρ^t represents the time correlation of the signals from the transmitters and ρ^r denotes the time correlation of the signals received by both receivers. Both are numbers from 0 to 1. The closer to 1, the lower the signal-to-noise ratio after demodulation at the receivers. Using these correlation coefficients, the impact factor of MIMO throughput due to time-domain correlation can be defined in the model as (in the format of decibels)

$$G_t = 10\lg\left(\sqrt[4]{(1-\rho^t)}\sqrt{(1-\rho^r)}\right). \quad (10)$$

In particular, when the channel has a linear behavior, the corresponding channel correlation matrix is symmetric, which indicates that $h_{1,2}(t) = h_{2,1}(t)$. In this case, (8) and (10) can be simplified as

$$\rho = \rho^t = \rho^r \quad (11a)$$

$$G_t = 7.5\lg(1-\rho). \quad (11b)$$

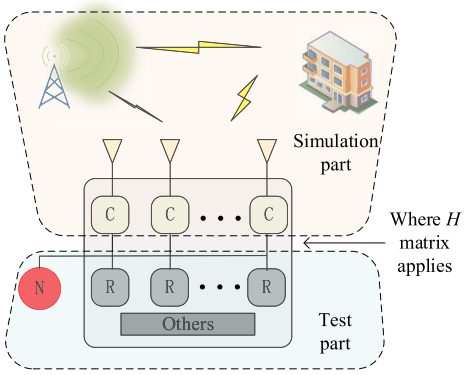

Fig. 5. Proposed half-test and half-simulation modeling method.

C. Half-Test and Half-Simulation Throughput Model

Fig. 4 shows the signal transmission and noise coupling under the practical operation of the MIMO UE, where the signals from the BS go through the BS antennas, the multipath channel, and the UE antennas, and finally, reach the receiver inputs. The half-test and half-simulation model are shown in Fig. 5, where the signals are simulated to obtain the channel correlation matrix $H(t)$, and a base throughput curve is obtained through an actual test while selecting a channel matrix. Finally, the throughput is computed when the DUT changes its orientation to the channel model by combining the simulations and measurements.

For a fixed UE, the base throughput curve is measured and denoted as a baseline, and its corresponding attenuation factor [defined in (5)], matrix normal number factor [defined in (6)], and time-domain correlation [defined in (10)] are denoted as $G_m^{\text{base}}, G_f^{\text{base}}$, and G_t^{base}, respectively. The change in the throughput curve with different channel correlation matrices (Fig. 6) is then given by

$$\Delta = \left(G_m^{ut} - G_f^{ut} - G_t^{ut}\right) - \left(G_m^{\text{base}} - G_f^{\text{base}} - G_t^{\text{base}}\right) \quad (12)$$

where G_m^{ut}, G_f^{ut}, and G_t^{ut} correspond to the factors in the other states to be tested and can be found via simulations. As mentioned earlier, the final 96 throughput curves can be obtained using one test plus 95 simulations.

D. Test Procedure

Based on the analysis in the previous two sections, the scheme proposed in this article theoretically requires only one test and multiple simulations to achieve a comprehensive performance evaluation. In reality, due to the existence of test uncertainties and the need to correct the model according to actual observations, the test procedure is specified as follows:

1) Calculate the corresponding channel correlation matrices for all test cases, which is feasible since the BS antenna

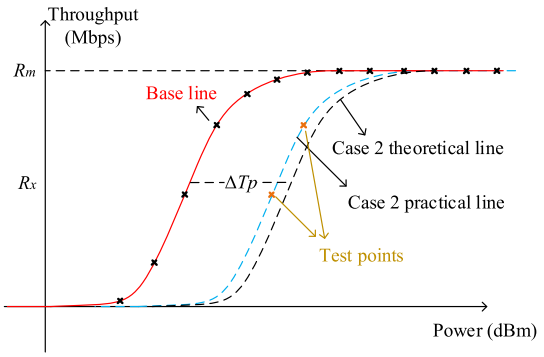

Fig. 6. Prediction of throughput performance for a second case, and prediction improvement using a small number of additional test points.

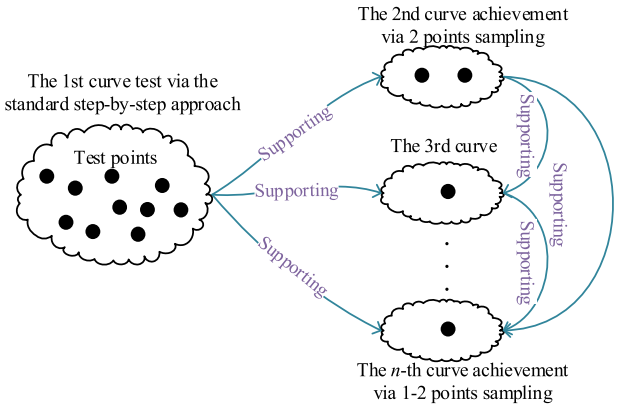

Fig. 7. With the improvement of measurement points, more and more samples will be used for prediction, resulting in improvement of the prediction accuracy of the model.

pattern, channel model, and terminal pattern are all known parameters.

2) Select a channel correlation matrix for throughput testing and use measured results for this case as a baseline. The test can be performed using either the RTS method or the MPAC method specified by the 3GPP standard. The theory and implementation of the RTS method are detailed in [5], [10], and [11], and the theory and experiments for the MPAC method are detailed in [15] and [16].
3) Calculate the difference between the throughput performance predicted by the model for a second test case and the baseline measurement, as given by (12). The simulation model can directly give the theoretical throughput-power curve for the second case as shown in Fig. 6 (the black dotted line). To account for model errors and base test uncertainties, however, one or two measurements should also be taken for the second case to yield an improved estimate as shown in Fig. 6 (the blue dotted line). It should be noted that these added test results can be obtained without a time-consuming searching process and only one or two test points are required, so they can be measured in about 40 s (for two test points) rather than the previous 5–8 min (for 15–24 test points in a general measurement curve according to the standards), thus giving a huge speed improvement.
4) After determining the second test curve, there are now two baselines that can be used for the prediction of the third curve, which obviously correspond to higher simulation accuracy. By increasing the number of test points, more and more samples provide base data for prediction, resulting in improved prediction accuracy of the model. As a result, as the testing progresses, fewer additional points are needed and the prediction accuracy quickly converges. The overall process is shown in Fig. 7.

IV. Validation

Validation results were obtained for several different MIMO UEs for comparison. The performance of each posture and orientation of the DUT was first measured using the 3GPP standard method as a reference. These results were then compared to the fast throughput measurement approach proposed

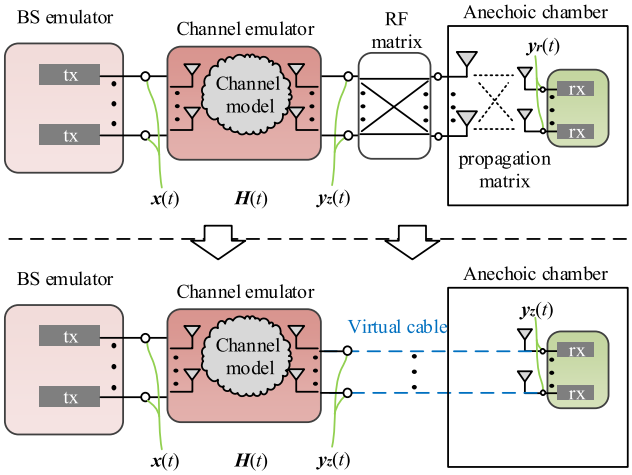

Fig. 8. Implementations of the RTS method.

in this article. The speed and accuracy of each method are compared in detail. The RTS method was utilized to measure the standard reference. The setups are outlined in Section IV-A.

A. Outline of the RTS Theory and Test Procedure

The RTS method is based on the first stage of DUT antenna pattern measurement, followed by the second stage of throughput measurement which combines the measured antenna pattern and the mathematical channel model in an instrument to generate the throughput test signals. The implementation of the RTS method is illustrated in Fig. 8, which is quoted from [29], which also details the RTS basic theory. By calculating the mathematical model in a channel emulator, the outputs of the channel emulator can be made to exactly reproduce $y_z(t) = H(t)x(t)$ defined in (1). The goal of the RTS implementation is to deliver the signal $y_z(t)$ into the receivers separately for MIMO testing. However, while the DUT is located in the chamber, the signal propagation between the chamber measurement antennas and the DUT receivers can be expressed as a matrix, denoted as a propagation matrix

Fig. 9. Validation system mainly includes an anechoic chamber and a BS emulator (integrating a channel emulator inside).

as shown in Fig. 8. To ensure the received signals $y_r(t)$ are equal to $y_z(t)$, an RF matrix is introduced which is the inverse of the propagation matrix. This way, the received signals at the MIMO receivers are ensured to be the channel emulator outputs, and also the desired test signals for the throughput measurement. This technique is also called the "virtual cable" method or "wireless cable" method, since the throughput test signals are actually delivered to the receivers from the channel emulator outputs without crosstalk over the air.

The RTS method was first published in [5]. The study [30] proposed a scheme to auto-solve the inverse matrix in an RTS test procedure. Later, an error analysis of RTS was performed in [29]. In 2022, a directly connected OTA measurement approach was developed based on RTS for an M by N (M, $N \geq 2$) MIMO OTA test [31]. The RTS methodology was incorporated into the standard by 3GPP in 2018 and CTIA in 2020 [10], [11].

B. Validation

To demonstrate the accuracy and speed of the proposed method, a test system was designed as shown in Fig. 9, where the BS emulator and channel emulator were integrated into one instrument, an E7515A from Keysight Technologies, and two cellular mobiles from Samsung and Google (the Samsung Tab2 and the Google Pixel xL) were utilized as the DUTs. The DUTs were located in an anechoic chamber, the RayZone 2800 from General Test System Inc. The SCME UMi channel model was selected for validation. It is one of only two standard models specified by 3GPP and CTIA for 4G long-term evolution (LTE) MIMO OTA tests. It will be expanded in the future for 5G MIMO throughput evaluations. Part of the parameters is listed in Table II. All protocol-related parameters can refer to 3GPP TS 37.544 and 3GPP test report 37.977.

In the experiments, two frequency points at different bands (751 MHz in band 13 and 2655 MHz in band 7) were tested for each DUT, eight postures were tested for each band (according to the 3GPP standard in Fig. 1), and 12 throughput-power curves were found for each posture. Consequently, a total of $2 \times 2 \times 8 \times 12 = 384$ results were produced to compare the test accuracy and speed. The protocol is specified as frequency division duplex (FDD) LTE. To quantify the performance of the proposed approach, the downlink power levels where the throughput was 50% of the maximum (see Fig. 3) were recorded as the MIMO performance indicator for both the fast measurement approach and for the reference, which is also recommended by the standards.

TABLE II
TEST PARAMETERS

Parameters	Value
Instruments	PC, RayZone 2800 from General Test System Inc., Keysight E7515A (base station plus channel emulator)
Test frequencies	751MHz (Band 13)
	2655MHz (Band 7)
Protocol and modulation	FDD-LTE
Max throughput	35.424 Mbps
DUT	Samsung Tab2 about 24cm × 17cm Google Pixel xL about 12cm × 17cm
Channel model	SCME UMi
Orientation	All the 8 portraits
Chamber size	3m×3m×3m
Test distance	1.24m
Number of test block	20000
Adjustment step of the downlink power	1dB

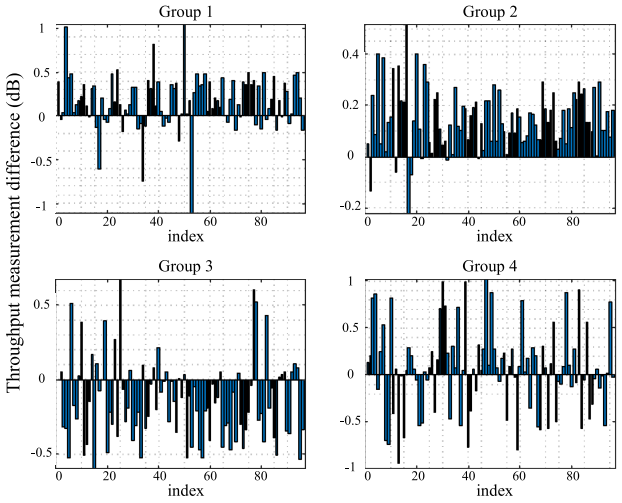

Fig. 10. Difference between the power levels required to achieve 50% of the maximum throughput as found using the proposed fast measurement approach and using the standard measurement technique.

C. Analysis

The difference between the power levels predicted by the fast approach and found in the reference measurements are shown in Fig. 10. The test results are divided into four groups, each corresponding to 96 throughput curve tests [8 (postures) × 12 (curves) = 96]. Group 1 corresponds to the

DUT of Samsung Tab2 under band 7, group 2 is the DUT of Google Pixel xl under band 7, group 3 corresponds to the DUT of Samsung Tab2 under band 13, and group 4 is the DUT of Google Pixel xl under band 13. All four groups followed the fast-testing process proposed in Section III, as shown in Fig. 7. Several conclusions can be drawn from these results:

1) The differences between the reference measurements and the fast measurement results are relatively small (all within ± 1.2 dB). Among the 384 comparisons, 91.93% are within ± 0.6 dB. This result demonstrates that the fast throughput model-based test method has a good correlation with practical test system measurements. It is worth noting that, as discussed earlier, the fast measurement results are obtained by first predicting throughput performance through calculations followed by a second step of improving estimates using one or two measurements at the predicated points. It is therefore not surprising that the accuracy has been maintained.
2) The effective test time used by the standard test method is about 39 h. When using the standard method, the UEs need to be recharged after 5–6 h of testing and then the communication link must be reestablished for testing. The charging time is not taken into account. The proposed fast method only requires about 3.1 h of testing, corresponding to a 12.6 times improvement of the test speed, without loss of test accuracy.

D. Discussion About Stability of the Model

The time-domain correlation coefficients ρ^t and ρ^r defined in (8) are real numbers between 0 and 1. Values of these correlation coefficients equal to 0 indicate that the signals are completely uncorrelated in the time domain, and the decoupling will not be disturbed. Values equal to 1 indicate that the signals are completely correlated, and the receiver cannot recover the originally transmitted signals regardless of the received power level, which also corresponds to the definition of G_t in (9).

In practical tests, when ρ^t or ρ^r approaches 1, the difference between the predicted results of the model and the actual test results may increase, due to the increase in the measurement uncertainty. For this case, it is necessary to add several more test points based on the predicted curve to improve the test accuracy. As in the process proposed in Section III, when ρ^t or ρ^r is larger than 0.85 (empirical value), it is suggested to increase the number of test points for verification to 2–4.

V. Conclusion

A semi-simulation semi-measurement-based MIMO throughput modeling scheme for wireless UE was proposed in this article, which can reduce the MIMO performance measurement time by more than a factor of ten without losing test accuracy. The fast measurement speed is obtained by first predicting throughput performance via calculations, followed by a second step of improving estimates via one or two practical measurements at the predicted points. Hundreds of experiments were conducted on two two-antenna-equipped DUTs to validate the approach. Results show that the method reduces a 39-h test to about 3.1 h without loss of accuracy.

A 2×2 MIMO is the basic configuration of most wireless portable terminals (e.g., IoT devices), which is the main scope of 3GPP and CTIA TSs [10], [11]. The proposed method is currently only applicable to 2×2 MIMO OTA testing. Nevertheless, we believe that the method opens up ideas for fast 4×4 MIMO testing, which is a topic of future research.

References

[1] J. G. Andrews et al., "What will 5G be?" *IEEE J. Sel. Areas Commun.*, vol. 32, no. 6, pp. 1065–1082, Jun. 2014, doi: 10.1109/JSAC.2014.2328098.

[2] L. Angrisani, D. Petri, and M. Yeary, "Instrumentation and measurement in communication systems," *IEEE Instrum. Meas. Mag.*, vol. 18, no. 2, pp. 4–10, Apr. 2015, doi: 10.1109/MIM.2015.7066676.

[3] L. Angrisani, A. Napolitano, and M. Vadursi, "Modeling and measuring link capacity in communication networks," *IEEE Trans. Instrum. Meas.*, vol. 59, no. 5, pp. 1065–1072, May 2010, doi: 10.1109/TIM.2009.2038304.

[4] Y. Gao, R. Ma, Y. Wang, Q. Zhang, and C. Parini, "Stacked patch antenna with dual-polarization and low mutual coupling for massive MIMO," *IEEE Trans. Antennas Propag.*, vol. 64, no. 10, pp. 4544–4549, Oct. 2016, doi: 10.1109/TAP.2016.2593869.

[5] W. Yu, Y. Qi, K. Liu, Y. Xu, and J. Fan, "Radiated two-stage method for LTE MIMO user equipment performance evaluation," *IEEE Trans. Electromagn. Compat.*, vol. 56, no. 6, pp. 1691–1696, Dec. 2014, doi: 10.1109/TEMC.2014.2320779.

[6] P. Shen, Y. Qi, W. Yu, J. Fan, and F. Li, "OTA measurement for IoT wireless device performance evaluation: Challenges and solutions," *IEEE Internet Things J.*, vol. 6, no. 1, pp. 1223–1237, Feb. 2019, doi: 10.1109/JIOT.2018.2868787.

[7] P. Shen, Y. Qi, W. Yu, J. Fan, Z. Yang, and S. Wu, "A decomposition method for MIMO OTA performance evaluation," *IEEE Trans. Veh. Technol.*, vol. 67, no. 9, pp. 8184–8191, Sep. 2018, doi: 10.1109/TVT.2018.2839726.

[8] *Technical Specification Group Radio Access Network; NR; Study on Test Methods*, 3GPP, document TR 38.810, Dec. 2018.

[9] *Spatial Channel Model for Multiple Input Multiple Output (MIMO) Simulations*, 3GPP, document TR 25.996 V13.0.0, Dec. 2015.

[10] *User Equipment (UE) Over the Air (OTA) Performance; Conformance Testing*, 3GPP, document TS 37.544 v14.5.0, 2018.

[11] *Test Plan for 2 × 2 Downlink MIMO and Transmit Diversity Over-the-Air Performance*, CTIA, Washington, DC, USA, Aug. 2016.

[12] J. F. Valenzuela-Valdes, A. M. Martinez-Gonzalez, and D. A. Sanchez-Hernandez, "Emulation of MIMO nonisotropic fading environments with reverberation chambers," *IEEE Antennas Wireless Propag. Lett.*, vol. 7, pp. 325–328, 2008, doi: 10.1109/LAWP.2008.928488.

[13] J. F. Valenzuela-Valdes, A. M. Martinez-Gonzalez, and D. A. Sanchez-Hernandez, "Diversity gain and MIMO capacity for nonisotropic environments using a reverberation chamber," *IEEE Antennas Wireless Propag. Lett.*, vol. 8, pp. 112–115, 2009, doi: 10.1109/LAWP.2008.2012279.

[14] X. Chen, P.-S. Kildal, J. Carlsson, and J. Yang, "Comparison of ergodic capacities from wideband MIMO antenna measurements in reverberation chamber and anechoic chamber," *IEEE Antennas Wireless Propag. Lett.*, vol. 10, pp. 446–449, 2011, doi: 10.1109/LAWP.2011.2152360.

[15] W. Fan, F. Zhang, and Z. Wang, "Over-the-air testing of 5G communication systems: Validation of the test environment in simple-sectored multiprobe anechoic chamber setups," *IEEE Antennas Propag. Mag.*, vol. 63, no. 1, pp. 40–50, Feb. 2021, doi: 10.1109/MAP.2019.2943305.

[16] W. Fan et al., "A step toward 5G in 2020: Low-cost OTA performance evaluation of massive MIMO base stations," *IEEE Antennas Propag. Mag.*, vol. 59, no. 1, pp. 38–47, Feb. 2017, doi: 10.1109/MAP.2016.2630020.

[17] Z. Wang, Z. Jiang, Z.-C. Hao, and W. Hong, "A novel probe selection method for MIMO OTA performance testing," *IEEE Antennas Wireless Propag. Lett.*, vol. 19, no. 12, pp. 2359–2362, Dec. 2020, doi: 10.1109/LAWP.2020.3033040.

[18] Y. Jing, Z. Wen, H. Kong, S. Duffy, and M. Rumney, "Two-stage over the air (OTA) test method for MIMO device performance evaluation," in *Proc. IEEE Int. Symp. Antennas Propag. (APSURSI)*, Jul. 2011, pp. 71–74, doi: 10.1109/APS.2011.5996385.

[19] M. Rumney, H. Kong, and Y. Jing, "Practical active antenna evaluation using the two-stage MIMO OTA measurement method," in *Proc. 8th Eur. Conf. Antennas Propag. (EuCAP)*, Apr. 2014, pp. 3500–3503, doi: 10.1109/EuCAP.2014.6902584.

[20] *Test Plan for Mobile Station Over the Air Performance*, CTIA, Washington, DC, USA, Oct. 2018.

[21] *Study on Radiated Metrics and Test Methodology for the Verification of Multi-Antenna Reception Performance of NR User Equipment (UE)*, 3GPP, document TR 38.827, 2020.

[22] *Study on Channel Model for Frequencies From 0.5 to 100 GHz*, 3GPP, document TR 38.901, 2019.

[23] *Verification of Radiated Multi-Antenna Reception Performance of User Equipment (UE)*, 3GPP, document TR 37.977, Sep. 2018.

[24] N. Zhang, P. Yang, J. Ren, D. Chen, Y. Li, and X. Shen, "Synergy of big data and 5G wireless networks: Opportunities, approaches, and challenges," *IEEE Wireless Commun.*, vol. 25, no. 1, pp. 12–18, Feb. 2018, doi: 10.1109/MWC.2018.1700193.

[25] E. Hossain and M. Hasan, "5G cellular: Key enabling technologies and research challenges," *IEEE Instrum. Meas. Mag.*, vol. 18, no. 3, pp. 11–21, Jun. 2015, doi: 10.1109/MIM.2015.7108393.

[26] S. Chen, J. Hu, Y. Shi, L. Zhao, and W. Li, "A vision of C-V2X: Technologies, field testing, and challenges with Chinese development," *IEEE Internet Things J.*, vol. 7, no. 5, pp. 3872–3881, May 2020, doi: 10.1109/JIOT.2020.2974823.

[27] M. T. Dao, V. A. Nguyen, Y. T. Im, S. O. Park, and G. Yoon, "3D polarized channel modeling and performance comparison of MIMO antenna configurations with different polarizations," *IEEE Trans. Antennas Propag.*, vol. 59, no. 7, pp. 2672–2682, Jul. 2011, doi: 10.1109/TAP.2011.2152319.

[28] P. Shen, Y. Qi, X. Wang, W. Zhang, and W. Yu, "A 2×2 MIMO throughput analytical model for RF front end optimization," *J. Commun. Inf. Netw.*, vol. 5, no. 2, pp. 194–203, Jun. 2020, doi: 10.23919/JCIN.2020.9130435.

[29] P. Shen, Y. Qi, W. Yu, and J. Fan, "UE reporting uncertainty analysis in radiated two-stage MIMO measurements," *IEEE Trans. Antennas Propag.*, vol. 69, no. 12, pp. 8808–8815, Dec. 2021, doi: 10.1109/TAP.2021.3090523.

[30] P. Shen, Y. Qi, W. Yu, and F. Li, "Inverse matrix autosearch technique for the RTS MIMO OTA test," *IEEE Trans. Electromagn. Compat.*, vol. 63, no. 4, pp. 962–969, Aug. 2021, doi: 10.1109/TEMC.2020.3029909.

[31] P. Shen, Y. Qi, W. Yu, F. Li, X. Wang, and X. Shen, "A directly connected OTA measurement for performance evaluation of 5G adaptive beamforming terminals," *IEEE Internet Things J.*, vol. 9, no. 16, pp. 15362–15371, Aug. 2022, doi: 10.1109/JIOT.2022.3150038.

Penghui Shen (Member, IEEE) received the B.S., M.S., and Ph.D. degrees in electronic information and technology from Hunan University, Changsha, China, in 2013, 2016, and 2020, respectively.

He is currently a Post-Doctoral Researcher with the Peng Cheng Laboratory, Shenzhen, China. His current research interests include single-in, single-out (SISO), multiple-input–multiple-output (MIMO), and 5G array measurements for wireless devices, electromagnetic compatibility (EMC), and antenna design.

Quan Yu (Fellow, IEEE) received the B.S. degree in radio physics from Nanjing University, Nanjing, China, in 1986, the M.S. degree in radio wave propagation from Xidian University, Xi'an, China, in 1988, and the Ph.D. degree in fiber optics from the University of Limoges, Limoges, France, in 1992.

He is currently a Research Professor with the Peng Cheng Laboratory, Shenzhen, China. His current research interests include the architecture of wireless networks and cognitive radio.

Dr. Yu is an Academician of the Chinese Academy of Engineering and the Founding Editor-in-Chief of the *Journal of Communications and Information Networks*.

Daryl G. Beetner (Senior Member, IEEE) received the B.S. degree in electrical engineering from Southern Illinois University, Edwardsville, IL, USA, in 1990, and the M.S. and D.Sc. degrees in electrical engineering from Washington University, St. Louis, MO, USA, in 1994 and 1997, respectively.

He is currently a Professor of electrical and computer engineering with the Missouri University of Science and Technology, Rolla, MO, USA (Missouri S&T), also the Former Chair of the ECE Department, Missouri S&T, the Director of the Electromagnetic Compatibility Laboratory, Missouri S&T, and the Director of the Center for Electromagnetic Compatibility, a National Science Foundation Industry/University Cooperative Research Center. He has authored more than 150 research articles, two book chapters, and multiple patents/invention disclosures, and received several best paper awards or nominations. His current research interests include a wide variety of topics including electromagnetic immunity and emissions from the integrated circuit to the system level.

Dr. Beetner was a recipient of the IEEE EMC Society Technical Achievement Award, in August 2020, and the IEEE-HKN C. Holmes MacDonald Outstanding Young Electrical Engineering Professor, in 2003. He has served the IEEE EMC Society as the University Grants Committee Chair, the SC-5 Special Committee on Power Electronics Secretary, the Educational Committee Secretary and the Vice-Chair, the Tutorials Chair, and as the TC-4 Electromagnetic Interference Control Secretary and served the IEEE as an Associate Editor for the IEEE TRANSACTIONS ON INSTRUMENTATION AND MEASUREMENT and as the Chair for the IEEE Medal for Environmental and Safety Technologies Selection Committee. He is the Former Chair of the Central States ECE Department Heads Association.

Yihong Qi (Fellow, IEEE) is a President and Chief Scientist of General Test Systems, Inc., Shenzhen, China, and a Founder at Pontosense Inc., Mercku Inc. Canada and Link-E, Zhuhai, China, and an Engineer, Scientist, Inventor, Entrepreneur, and a Research Professor with the Peng Cheng Laboratory, Shenzhen, and an Honorary Professor at Xidian University and Southwest Jiaotong University. He is also an Adjunct Professor at the EMC Laboratory, Missouri University of Science and Technology, Rolla, MO, USA, Western University, Ontario, Canada, Dalian Maritime University, China. He is an Inventor of more than 500 published and pending patents. He has published more than140 academic papers. His smartphone antenna design patent significantly reduced harmful radio-wave radiation to the human head, which could potentially help billions of smartphone users reduce potential hazardous electromagnetic radiation. His invention also resolved the hearing aid compatibility issue; there are more than 20-million cell phone users who depend on hearing aid devices. His standards related inventions has have made the certification process for 4G, 5G, and potentially 6G wireless communications and autonomous cars more efficient and coeffective. From 1995 to 2010, he was with Research in Motion (Blackberry), Waterloo, ON, where he was the Director of Advanced Electromagnetic Research.

Dr. Qi is a Fellow of Canadian Academy of Engineering, National Academy of Inventors, and the Asia-Pacific Artificial Intelligence Association. He was a Distinguished Lecturer of IEEE EMC Society. He was founding Chairman of the IEEE EMC society TC-12. He is an Associate Editor of IEEE INTERNET OF THINGS JOURNAL and IEEE TRANSACTIONS ON ELECTROMAGNETIC COMPATIBILITY. He has received an IEEE EMC Society Technical Achievement Award. His inventions won 2019, 2020 CES innovation awards, 2021 CES Network Product award, 2022 CES Wellbeing Product award, Red Dot award IEEE HI-TC industrial award among other awards.